Published in final edited form as:
Magn Reson Imaging. 2013 June ; 31(5): 783–788. doi:10.1016/j.mri.2012.11.005.

Measurements of RF Heating during 3.0T MRI of a Pig Implanted with Deep Brain Stimulator

Krzysztof R Gorny, PhD[1], **Michael F Presti, MD, PhD**[2], **Stephan J Goerss**[3], **Sun C Hwang, MD, PhD**[3], **Dong-Pyo Jang, PhD**[3], **Inyong Kim, MD, PhD**[3], **Yunhong Shu, PhD**[1], **Christopher P Favazza, PhD**[1], **Kendall H Lee, MD, PhD**[3], and **Matt A Bernstein, PhD**[1]

[1]Department of Radiology, Mayo Clinic, Rochester, MN

[2]Department of Neurology, Mayo Clinic, Rochester, MN

[3]Department of Neurologic Surgery, Mayo Clinic, Rochester, MN

Abstract

Purpose—To present preliminary, in vivo temperature measurements during MRI of a pig implanted with a deep brain stimulation (DBS) system.

Materials and Methods—DBS system (Medtronic Inc., Minneapolis, MN) was implanted in the brain of an anesthetized pig. 3.0T MRI was performed with a T/R head coil using the low-SAR GRE EPI and IR-prepped GRE sequences (SAR: 0.42 W/kg and 0.39 W/kg, respectively), and the high-SAR 4-echo RF spin echo (SAR: 2.9 W/kg). Fluoroptic thermometry was used to directly measure RF-related heating at the DBS electrodes, and at the implantable pulse generator (IPG). For reference the measurements were repeated in the same pig at 1.5T and, at both field strengths, in a phantom.

Results—At 3.0T, the maximal temperature elevations at DBS electrodes were 0.46 °C and 2.3 °C, for the low- and high-SAR sequences, respectively. No heating was observed on the implanted IPG during any of the measurements. Measurements of in-vivo heating differed from those obtained in the phantom.

Conclusion—The 3.0T MRI using GRE EPI and IR-prepped GRE sequences resulted in local temperature elevations at DBS electrodes of no more than 0.46°C. Although no extrapolation should be made to human exams and much further study will be needed, these preliminary data are encouraging for the future use 3.0T MRI in patients with DBS.

Keywords

MRI; fMRI; medical device safety; DBS; Deep Brain Stimulation; 3.0T

1. Introduction

Deep brain stimulation (DBS) is an FDA-approved neurosurgical therapy for the treatment of Parkinson's disease [1,2], essential tremor [3], dystonia [4], or treatment-resistant depression [5]. The DBS system (see Figure 1a) consists of the implantable pulse generator (IPG) and flexible lead(s) with electrodes housed at the tips. The stimulating leads are

implanted in an anatomical target within the brain (e.g., subthalamic nucleus) and subcutaneously connected to the IPG commonly anchored in an ipsilateral subclavicular location. During stimulation, the IPG generates electric pulses that are delivered to the targeted neural structures, often resulting improvement of neurological symptoms.

MRI provides plays a key role in DBS implantation, both during surgical planning as well as post-operative confirmation of target lead placements. At 1.5T, MRI of DBS is considered to be conditionally safe under controlled imaging conditions and careful monitoring of patients [6–10]. The current manufacturer's guideline (applies to Medtronic devices only) specifies that the clinical MRI scanning of DBS patients may be performed only at field strengths of 1.5T, using a transmit-receive (T/R) head coil, limiting the average head specific absorption rate (SAR) to 0.1 W/kg, and with the IPG output zeroed and switched off [11,12]. Deviation from these conditions may lead to potentially harmful radio frequency (RF)–heating of implanted DBS components (temperature elevations of up to 59.1°C have been observed in phantom studies [13]) and result in serious patient injury [9, 14,15].

At present, relatively little is known about the exact neurobiological mechanisms underlying DBS therapy. Functional MRI (fMRI), and particularly fMRI performed at 3.0T (the field strength of choice for high resolution brain MRI), could potentially become instrumental in identifying DBS-induced alterations to neural activity, which are responsible for either the beneficial of adverse response to the therapy. Given the current manufacturer safety guidelines however, assessment the RF-heating related to 3.0T fMRI-relevant sequences is of interest from the perspective of patient safety. RF-heating around DBS electrodes during 3.0T fMRI has previously been the subject of phantom investigations [16,17,18]. The maximal temperature increases due to fMRI–relevant sequences were found to be below 1.36 °C.

In this work, in-vivo local temperature increases near DBS electrodes were measured directly during 3.0T MRI scanning of anesthetized pig. The DBS electrodes were implanted in the basal ganglia of the animal and measurements were performed both with and without the DBS stimulus, and for multiple orientations of pig's head within the scanner. The standard clinical imaging pulse sequences were played for each experimental configuration: two relatively "low-SAR" sequences used for fMRI and planning of DBS implantation, and one relatively "high-SAR" sequence. Reference heating measurements were also performed in the same pig at 1.5T field strength, and at both field strengths in a phantom.

2. Methods

Fluoroptic thermometers (0.8mm-tip, STF-2, MR-conditional Model 750 system, Lumasens, Santa Clara, CA) were used to measure, in real-time, temperature elevations during MRI scanning. Probes 1 and 2 were attached directly to the proximal and the distal electrodes of the DBS system (DBS electrodes model 3389, Soletra IPG, model 7426, Medtronic Inc., Minneapolis, MN), as shown in Figure 1. Firm attachment was achieved using surgical tethers and superglue.

Animal anesthesia was performed under an Institutional Animal Care and Use Committee-approved protocol. The pig was initially sedated with Telazol (5 mg/kg i.m.) and Xylazine (2 mg/kg i.m.), followed by intubation. Sedation was maintained with a solution of 1.5–3% isoflurane during surgery and 1.5–2% isoflurane during MRI. The vital signs (heart rate: 120 bpm, respiration rate: 12/min, and temperature: 36–37° C) were continuously monitored throughout the procedure. The implantation was performed using a custom MRI-compatible stereotactic pig head holder that is a hybrid of the traditional Kopf animal stereotactic device (David Kopf Instruments, Tujunga, CA) and the Leksell human stereotactic system (Elekta, Stockholm, Sweden). The head holder uses the Kopf micropositioners and/or the Leksell

arc-quadrant to deliver probes and electrodes. The COMPASS® Surgical Planning device (Compass International, Inc., Rochester, MN) used to plan human procedures was modified to perform the same planning steps using the custom pig frame. The DBS electrodes with Probes 1 and 2 attached were implanted in the STN (Figures 2a and 2b). To account for anesthesia-induced change in brain temperature [21,22,23] and RF-heating of bulk tissues, Probe 3 was placed in the contralateral position, approximately 10 mm from the DBS lead tip (Figures 2a and 2b). The IPG (Probe 4) was implanted in the prone pig's back to simulate the placement in a supine human's chest. The DBS system was surgically placed by a team experienced in performing of such procedures in both patients as well as animal studies. The DBS leads were inserted into the pigs head at a substantial angle (in the superior-posterior direction) so that their orientation during MRI was as analogous as possible to that used in humans, given the substantial anatomical differences. The lead length and path were also selected to match as closely as possible those used during human implantations.

The 3.0T and 1.5T scanning (GE Healthcare, 14.0 M4 software) was performed with the pig's head secured within the head holder inside the manufacturers standard transmit/receive head coils (GE Healthcare: 3.0T Split Head Coil, model 2376114 and 1.5T Quad Head Coil, model 46-28211862). Five separate measurements (runs) were performed at 3.0T. The first and second runs were performed with the IPG stimulation switched off. The third run was performed with the IPG stimulation switched on. During the fourth and the fifth runs, in addition to IPG stimulation being switched on, the pig's head was shifted by 2 cm along the z- direction, and rotated by 3° inside the imaging coil, respectively. Three different 7-minute pulse sequences were played per each run: RF spin-echo with 4-echoes ("4-echo"), 3D inversion recovery fast spoiled gradient recalled echo ("IR-FSPGR", analogous to MP-RAGE used on other manufacturers' systems, and used for pre-surgical DBS planning and post-surgical assessment), and gradient-recalled echo EPI ("fMRI," used for functional MRI studies). The relevant sequence parameters were: 4-echo, TR/TE1/TE2/TE3/TE4 100/20/40/60/80ms, 256×256 matrix, a single 3mm-slice, 7min 19s scan time; IR-FSPGR, TR/TE/TI 6.6/3/400ms (3.0T) and 7.3/3/400 (1.5T), 256×256 matrix, 11° flip angle, 130 slices per slab, 7min 2s scan time; fMRI, TR/TE 2700/30ms, 64×64 matrix, 90° flip angle, slice thickness 3.3mm, 44 slices, 7min 2s scan time. A cooling interval of 5 minutes was allowed between each pulse sequence run. For each sequence, the root-mean-squared values of B_1^+ averaged over one TR period, were calculated (see Table 1).

When switched on, the IPG was set to generate 3.5 V pulses of 60 microsecond width, with frequency of 1.85 Hz. During runs with IPG switched on, after completion of each imaging sequence, the table with the animal was moved outside the scanner room where hand-held N'Vision Clinician Programmer (Model 8840, Medtronic Inc., Minneapolis, MN) was used to interrogate and reset, if needed, the operational status of the IPG. Following the five 3.0T runs, the animal was transferred to the 1.5T scanner suite where an additional run was performed. The following data were recorded: scanner-displayed (i.e., predicted) average coil SAR, the plateau value of the real-time power monitor's 6-minute average (available on 3.0T only), and the auto-prescan power level or transmit gain (TG, in units of 0.1 dB) corresponding to each sequence.

On both 1.5T and 3.0T MR systems used in this investigation, the predicted average head coil SAR is displayed on the operator's console following the entry of the patient weight and the pulse sequence parameters. Additionally, the 3.0T scanner displays the 10-second and 6-minute moving average of a real-time power monitor during the course of the scan. The scanner's SAR predictions are modeled using the value of entered patient weight, assuming typical human anatomy and the RF output (i.e., TG) established in auto pre-scan provides the desired flip angles. Therefore, the value of the average head SAR displayed on the MR scanner during the animal experiment was the value expected for a human weighing 31 kg,

rather than the 31 kg pig. To better approximate the actual average coil SAR deposited in the pig a correction factor was determined empirically using the previously described calorimetric method [19] as follows: 1. auto-prescan values of TG as a function of patient weight were recorded on 13 human volunteers at 1.5T and 3.0T under an IRB-approved protocol for each of the pulse sequences used in the animal experiment, 2. volunteer data were fitted with a linear-least squares method and the patient weights corresponding to the auto-prescan TG applied in the animal experiment were determined, 3. these patient weights were then entered into the MR scanner to determine corrected SAR values. The SAR values (corrected and displayed) are shown in Table 1. Additionally, at 3.0T, the insulated head phantom was used to directly measure the average coil SAR according to methods described elsewhere [19].

To calculate the MRI-induced temperature elevations, data from Probes 1, 2, and 3 were first corrected for the overall brain temperature decrease due to anesthesia measured by Probe 3. Second, the baseline temperatures corresponding to execution of any of the imaging sequence were computed by averaging over 120 seconds before the start of the sequence. The maximal temperature elevations relative to the baselines were subsequently found.

For reference, measurements of RF-induced heating during 3.0T and 1.5T MRI scanning were acquired in a human trunk-and-head phantom filled with polyacrlic gelled saline solution [20]. The DBS device with the attached fluoroptic thermometers were placed inside the phantom at locations corresponding to those in the pig, see Figure 2a. Following setup, the phantom was allowed to thermally stabilize prior to testing: 12 hours for the 3T measurements, and 2 hours for the 1.5T measurements. The IR-FSPGR, fMRI, and 4-echo pulse sequences were executed in the same manner as in the animal experiment, and the corresponding temperature elevations were recorded. For each sequence, TG value was established during the auto pre-scan, and both patient weight and the corresponding SAR were found based on volunteer results, as described above ($B^{+}_{1,rms}$ and SAR are shown in Table 1). During the phantom measurements the IPG was turned off.

The phantom setup was also used to investigate heating around DBS electrodes due to stimulus alone. With the phantom inside the scanner, the DBS leads were connected to the external IPG (Model 3628, electrodes Model 3389; Medtronic Inc.) located outside the scanner room (in the operator area). Two consecutive 5-minute temperature measurements were performed with the stimulus on and with the stimulus off. The measurements were then repeated during two executions of IR-FSPGR sequence using body coil for RF transmit (with and without the stimulus).

3. Results

A sample temperature history recorded in-vivo during one of the runs at 3.0T is shown in Figure 3. Data shown are corrected for the systematic, −0.35 °C/hour, decrease of brain temperature due to anesthesia measured at the contralateral position (Probe 3). At both field strengths pronounced and rapid heating effects of MRI scanning were seen near the DBS electrodes, where 80% of the total temperature rise occurred during the first 30 seconds after the start of the acquisition. No statistically significant difference was found between temperature increases measured at the two electrodes ($P = 0.63$). The maximal temperature elevations measured at DBS electrodes during 3.0T scanning are listed in Table 2.

We observed a 26% increase in temperature elevations induced by the 4-echo sequence for run 3 compared to runs 1 and 2, which could be attributed to switching the IPG stimulus on. However, no such difference was found corresponding to the low-SAR sequences. With the IPG stimulus on, rotating the pig's head had the most pronounced effect on the heating,

which further increased by additional 12% for the 4-echo and nearly doubled for the low-SAR sequences. Due to the limited number of measurements, no statistical significance can be established from these data.

The summary of in-vivo measurements, at both field strengths, is provided in Table 3. The corresponding phantom data are shown in Table 4. In the phantom, the temperature elevations measured at the distal electrode were consistently higher than those measured at the proximal electrode: by 0.14 and 0.05 °C, at 3.0T and 1.5T, respectively. However, since only one run was performed at each field-strength, this trend could not be reliably verified. No heating was observed on the IPG in any of the measurements.

The temperature increases at the contralateral location were non-negligible only during executions of the 4-echo sequence, both during the in-vivo and the phantom experiments. These data are shown in Table 5. Unlike in the case of the electrode heating, temperatures at the contralateral location gradually increased over time during scanning, representing tissue heating due to bulk deposition of RF-energy.

If placed in the “on” state at the beginning of the scan, the IPG operation was consistently shut off during execution of the IR-FSPGR and 4-echo sequences, at both field strengths. At 3.0T, fMRI sequence interrupted IPG operation in 1 out of 3 executions. No change in the on/off state was seen during the single fMRI execution at 1.5T.

Temperature measured at a distal electrode in a head-and-trunk phantom was 17.33±0.03°C with stimulus on versus 17.31±0.02°C with stimulus off. During IR-FSPGR no difference between temperatures rises with and without stimulus were observed (0.02±0.04°C).

4. Discussion

The maximal temperature rises associated with 3.0T fMRI and IR-FSPGR sequences measured around the DBS electrodes implanted in the in-vivo pig brain were 0.44 and 0.46° C, respectively. The existing guidelines [24,25] use 1.0° C as the maximum allowable temperature rise in the brain which provides a sufficient safety margin to avoid adverse effects. The guidelines apply to bulk RF-heating of tissues, however 1.0° C has been used previously as a reference for RF-heating of DBS leads in-vitro (at 9.4T) in a pig model [26]. Implant heating during MRI is usually more rapid than the corresponding bulk heating, which could pose additional concerns given the in-vivo evidence that increased heating rates enhances the degree of cytotoxicity and lowers temperature thresholds for tissue kill [27]. We therefore find it encouraging that the sequences associated with 3.0T fMRI induced temperature rises below the very conservative value of 1.0° C, both in the pig and in the phantom. Executions of the high-SAR, 4-echo RF spin echo, however, resulted in temperature rises well above 1.0° C, which further illustrates need for caution during selection of appropriate pulse sequences for scanning DBS patients.

While the average coil SAR is useful as a clinical predictor of RF-induced bulk tissue heating, it is an unreliable predictor of RF heating near the DBS implants [28]. Despite this limitation, the SAR estimates are often used by manufacturers of implanted devices in guidelines for the scanning of MR-conditional devices. The SAR estimates are sometimes augmented by providing estimated values of $B^{+}_{1,rms}$, which can provide a more standardized (across vendors) characterization of the applied RF field since it is independent of the specific model a vendor employs to estimate SAR. Both SAR and $B^{+}_{1,rms}$ estimates, however, are only surrogate measures for temperature increase. Consequently, direct measurements, in-vitro and in-vivo, of local temperature elevations near DBS implants can yield valuable information, particularly when acquired in conjunction with SAR and $B^{+}_{1,rms}$ estimates. For

these reasons, we supplemented the scanner-supplied, predicted SAR values with real-time power monitor measurements (available at 3.0T only), SAR values corrected by the calorimetric method of [19], and expected values of root-mean-square (rms) average of RF-field $B^{+}_{1\,\mathrm{rms}}$ corresponding to each sequence. At 3.0T, additional calorimetric measurements were performed to measure SAR directly. Data in Table 1 show that displayed average coil SAR (subscript D) deviates from the values measured, either with calorimetry or the power-monitor. We believe these results reaffirm the value of direct method of measuring SAR, especially because the SAR-calculating algorithms vary across MRI platforms from different manufacturers and are prone to errors depending on “patient” weight entered in phantom or animal studies.

The average head coil SAR corresponding to imaging sequences executed at 3.0T was higher than that for the same sequences executed at 1.5T. This corresponded well with the 3.0T versus 1.5T temperature elevations measured at the contralateral location in pig’s brain and in the phantom experiments. In contrast, the in-vivo heating at DBS electrodes did not follow the increase in head SAR (Table 3). In fact, for the 4-echo, the heating at 3.0T was lower than at 1.5T, and remained approximately unchanged for the IR-FSPGR. Additionally, the DBS heating measured in the phantom was generally lower than that in the animal (especially at 1.5T). We speculate that, given the lack of perfusion in the phantom, this finding may be attributed to the fact that the heating around the DBS electrodes depends not only on SAR but also on local nonuniform distributions of electric fields and on the details of lead placement [13,14]. The differences between the phantom and the animal measurements illustrate that in-vivo experiments can provide new information, but we also emphasize extreme caution is required when generalizing or extrapolating limited data.

While the measurements of RF-implant heating performed in phantoms remain the standard assessment method, we think the additional in-vivo measurements can supplement phantom data by accounting for the effects of perfusion or heterogeneous distributions of tissue conductivities, and variations in the resulting SAR distributions [29,30].

The 4-echo and IR-FSPGR sequences interrupted the function of the IPG (3 runs at 3.0T and 1 run at 1.5T). This was attributed solely to executions of the pulse sequences, since moving the animal with the implanted IPG into and out of the bore had no effect on the on/off state of the DBS. The fMRI sequence interrupted the IPG one out of three times at 3.0T and had no effect on the IPG during a single execution at 1.5T. Similar findings related to interruption of IPG function by MRI sequences (1.5T) were reported previously [13, 31].

Both switching the IPG stimulus on and varying the orientation of implanted DBS leads inside the MRI scanner affected temperature elevations around the DBS electrodes. Based on our data in-vivo, we cannot reliably separate the two effects, due to the limited number of runs performed (which is a limitation of this work) and further experiments are needed to separate the two contributions and establish their impact on DBS heating. Our phantom experiment at 1.5T found no evidence of DBS electrode heating due to DBS stimulus alone (with or without the MRI) which seems to indicate that the lead orientation within the scanner plays a major role in the extent of RF implant heating.

The in-vivo study presented in this note is preliminary and has limitations, particularly in its use of only a single animal. Porcine model is additionally limited due to significant anatomical differences between the pig and human, which can lead to differences of RF field coupling to tissue. On the other hand, the thermal conductivities of tissues within porcine head are very similar to those of a human [26, 32] and therefore, despite its limitations, the porcine model has been considered as appropriate for studies of the effects of RF-heating

[33], and in-vitro and in-vivo studies in the porcine model at 9.4T have recently been published [26,34].

Our measurements may also be considered as limited in that they were performed on anesthetized animal. The isoflurane, which is a well known vasodilator, has been reported to decrease the core temperature by 1~1.5°C during the first hour and decrease it slowly and linearly for the next 2~3h [21–23]. Additionally, the vasodilation effect of isoflurane affects the cerebral blood flow and metabolic rate [24] and reduces the baseline brain temperature, which in our case was shown to be −0.35 °C/h, which is consistent with the previous reports [24] and represents anesthesia-induced mild hypothermal effect (−1~3°C). We attempted to minimize this phenomenon by maintaining and monitoring the vital signs (heart rate: ~120 bpm, respiration rate: 12/min) and use of a circulating water blanket to keep the body temperature at 36–37 °C. The brain temperature drift of −0.35 °C/hour we observed during the experiment contralateral to the lead corresponds to a temperature change of about −0.05 °C during an 8-minute MRI, which is substantially lower in magnitude than the rapid RF-heating of DBS leads, and is below the sensitivity of our thermometers. Additionally, the fiberoptic thermometers were in close contact with the DBS electrodes (Figure 1). At these locations the heating was dominated by the coupling of the DBS leads to the RF-fields and not by the relatively slow changes to brain metabolism induced by anesthesia.

Other limitations of this study include: sensitivity of the temperature rise to the details of lead placement [18] or their position inside the scanner [35], and dependence of the measurements on exact geometry of temperature probe orientation [36]. Because of these limitations, the data presented in this note are not sufficient to draw any general conclusions regarding safety of patients during fMRI studies performed at 3.0T. It is also important to stress that we used T/R head coils for our imaging. Use of body-coil transmit would result in additional heating, and is outside the scope of this investigation. Much caution must be exercised when extrapolating these results, especially across different MRI platforms [29, 37], and the authors encourage further testing prior to changing any safety recommendations.

5. Conclusions

The preliminary data presented in this note are, to our knowledge, the first direct, in vivo temperature measurements reported on 3.0 T MRI with implanted DBS. 3.0T MRI using low-SAR fMRI and IR-FSPGR sequences resulted in local temperature elevations at DBS electrodes, both in vivo and in a phantom, of no more than 0.3 °C. These data are highly specific to the particular MRI systems (GE) and DBS device (Medtronic) used our tests. Although no generalization or extrapolation should be made to human exams and much further study will be needed, these preliminary data are encouraging for the future use 3.0T MRI in patients with DBS.

Acknowledgments

The authors would like to acknowledge Paul H Min, PhD for useful discussions and contribution to details pertaining to animal anesthesia.

This work was supported by the following National Institute of Health grants: K08 NS 52232 and R01 NS 70872.

References

1. Lozano AM, Dostrovsky J, Chen R, Asby P. Deep brain stimulation for Parkinson’s disease: disrupting the disruption. Lancet Neurol. 2002; 1:225–31. [PubMed: 12849455]

2. Bronstein JM, Tagliati M, Alterman RL, et al. Deep brain stimulation for Parkinson disease: an expert consensus and review of key issues. Arch Neurol. 2011; 68:165. [PubMed: 20937936]
3. Flora ED, Perera CL, Cameron AL, Maddern GJ. Deep brain stimulation for essential tremor: a systematic review. Mov Disord. 2010; 25:1550–59. [PubMed: 20623768]
4. Ostrem JL, Racine CA, Glass GA, et al. Subthalamic nucleus deep brain stimulation in primary cervical dystonia. Neurology. 2011; 76(10):870–8. [PubMed: 21383323]
5. Mayberg HS, Lozano AM, Noon V, et al. Deep brain stimulation for treatment-resistant deppression. Neuron. 2005:45-651-660. [PubMed: 16202708]
6. Chhabra V, Sung E, Mewes K, et al. Safety of magnetic resonance imaging of deep brain stimulator systems: a serial imaging and clinical retrospective study. J Neurosurg. 2010; 112:497–502. [PubMed: 19681685]
7. Fraix V, Chabardes S, Krainik A, et al. Effects of magnetic resonance imaging in patients with implanted deep brain stimulation systems. J Neurosurg. 2010; 113:1242–5. [PubMed: 20187699]
8. Aziz TZ. Current and future directions of post-deep brain stimulation implant magnetic resonance imaging scanning. World Neurosurg. 2011; 76:69–70.
9. Zrinzo L, Yoshida F, Hariz M. World Neurosurg. 2011; 76:164–172. [PubMed: 21839969]
10. Ullman M, Vedam-Mai V, Krock N, et al. A pilot study of human brain tissue post-magnetic resonance imaging: information from the National Deep Brain Stimulation Brain Tissue Network (DBS-BTN). Neuroimage. 2011; 54:S233–S237. [PubMed: 20849960]
11. Medtronic, Inc. [Last accessed March 28, 2012.] MRI Guidelines for Medtronic Deep Brain Stimulation Systems. 2010. Available at: http://professional.medtronic.com/wcm/groups/mdtcom_sg/@mdt/@neuro/documents/documents/dbs-mri-gdlns.pdf
12. Larson PS, Richardson RM, Starr PA, Martin AJ. Magnetic resonance imaging of implanted deep brain stimulators: experience in large series. Stereotact Funct Neurosurg. 2008; 86:92–100. [PubMed: 18073522]
13. Georgi J–C, Stippich C, Tronnier VM, Heiland S. Active deep brain stimulation during MRI: A feasibility study. Magn Reson Med. 2004; 51:380–88. [PubMed: 14755664]
14. Spiegel J, Fuss G, Backens M, et al. Transient dystonia following magnetic resonance imaging in a patient with deep brain stimulator electrodes for the treatment of Parkinson's disease. J Neurosurg. 2003; 99:772–774. [PubMed: 14567615]
15. Henderson JM, Tkach J, Phillips M, Baker K, Shellock FG, Rezai AR. Permanent neurological deficit related to magnetic resonance imaging in a patient with implanted deep brain stimulation electrodes for Parkinson's disease: case report. Neurosurgery. 2005; 57(5):E1063. [PubMed: 16284543]
16. Phillips MD, Baker KB, Lowe MJ, et al. Parkinson disease: pattern of functional MR imaging activation during deep brain stimulation of subthalamic nucleus-initial experience. Radiology. 2009; 239:209–216. [PubMed: 16567487]
17. Carmichael DW, Pinto S, Limousin-Dowsey P, et al. Functional MRI with active, fully implanted, deep brain stimulation systems: safety and experimental confounds. Neuroimage. 2007; 37(2): 508–17. [PubMed: 17590355]
18. Rezai AR, Finelli D, Nyenhuis JA. Neurostimulation systems for deep brain stimulation: in vitro evaluation of magnetic resonance-related heating at 1. 5 tesla. J Magn Reson Imaging. 2002; 15:241–250. [PubMed: 11891968]
19. Gorny KR, Bernstein MA, Felmlee JP, et al. Calorimetric calibration of head SAR estimates displayed on a clinical MR scanner. Phys Med Biol. 2008; 53:2565–2576. [PubMed: 18441413]
20. ASTM Standard F2182. 2011a: Standard test method for measurement of radio frequency induced heating near passive implants during magnetic resonance imaging. American Society for Testing and Materials (ASTM) International; West Conshohocken, PA: 2002. www.astm.org
21. Kurz A, Sessler DI, Christensen R, Dechert M. Heat balance and distribution during the core temperature plateau in anesthetized humans. Anesthesiology. 1995; 83:491–499. [PubMed: 7661349]
22. Michenfelder, J. Anesthesia and the Brain: Clinical, Functional, and Vascular Correlates. New York: Churchill Livingstone; 1988.

23. Erickson KM, Lanier WL. Anesthetic technique influences brain temperature, independently of core temperature, during craniotomy in cats. Anesth Analg. 2003; 96(5):1460–6. [PubMed: 12707150]
24. Kahveci FS, Kahveci N, Alken T, et al. Propofol versus isoflurane anesthesia under hypothermic conditions: effects on intracranial pressure and local cerebral blood flow under diffuse traumatic brain injury in the rat. Surg Neurol. 2001; 56(3):206–14. [PubMed: 11597656]
25. International Electrotechnical Commission (IEC). Medical electrical equipment – Particular requirements for the safety of magnetic resonance equipment for medical diagnosis. 2002 IEC 60601-2-33, 1995 revised 2002
26. International Commission on Non-Ionizing Radiation Protection (ICNIRP). On medical magnetic resonance procedures: protection of patients. Health Physics. 2004; 87(2):197–216. [PubMed: 15257220]
27. Shrivastava D, Abosch A, Hanson T, et al. Effect of the extracranial Deep Brain Stimulation lead on radiofrequency heating at 9.4 Tesla (400. 2 MHz). J Magn Reson Imaging. 2010; 32:600–607. [PubMed: 20815057]
28. Herman TS, Gerner EW, Magun BE, et al. Rate of heating as a determinant of hyperthermic cytotoxicity. Cancer Res. 1981; 41:3519–23. [PubMed: 7260914]
29. Baker KB, Tkach JA, Phillips MD, Rezai AR. Variability in RF-induced heating of deep brain stimulation implant across MR systems. J Magn Reson Imaging. 2006; 24:1236–1242. [PubMed: 17078088]
30. Collins CM, Li S, Smith MB. SAR and B_1 field distributions in a heterogeneous human head model within a birdcage head coil. Magn Reson Med. 1998; 40:847–56. [PubMed: 9840829]
31. Collins CM, Wang Z. Calculation of radiofrequency electromagnetic fields and their effects in MRI of human subjects. Magn Reson Med. 2011; 65:1470–82. [PubMed: 21381106]
32. Rezai AR, Lozano AM, Crawley AP, et al. Thalamic stimulation and functional magnetic resonance imaging: localization of cortical and subcortical activation with implanted electrodes. J Neurosurg. 1999; 90:583–90. [PubMed: 10067936]
33. Dewhirst MW, Viglianti BL, Lora-Michiels M, et al. Basic principles of thermal dosimetry and thermal thresholds for tissue damage from hyperthermia. Int J Hyperthermia. 2003; 19:267–294. [PubMed: 12745972]
34. Shrivastava D, Hanson T, Kulesa J, et al. Radio-frequency heating at 9. 4T-in vivo thermoregulatory response in swine. Magn Reson Med. 2009; 62:888–895. [PubMed: 19572392]
35. Nordbeck P, Ritter O, Weiss I, et al. Impact of imaging landmark on the risk of MRI-related heating near medical implanted devices like cardiac pacemaker leads. Magn Reson Med. 2011; 65:44–50. [PubMed: 20806352]
36. Mattei E, Triventi M, Calcagnini G, et al. Temperature and SAR measurement errors in the evaluation of metallic linear structures heating during MRI using fluoroptic probes. Phys Med Biol. 2007; 52:1633–46. [PubMed: 17327653]
37. Kainz W. Response to Shellock et al. Vagus nerve stimulation therapy system: in vitro evaluation of magnetic resonance imaging-related heating and function at 1. 5 and 3 Tesla. Neuromodulation. 2007; 10:76–77. [PubMed: 22151815]

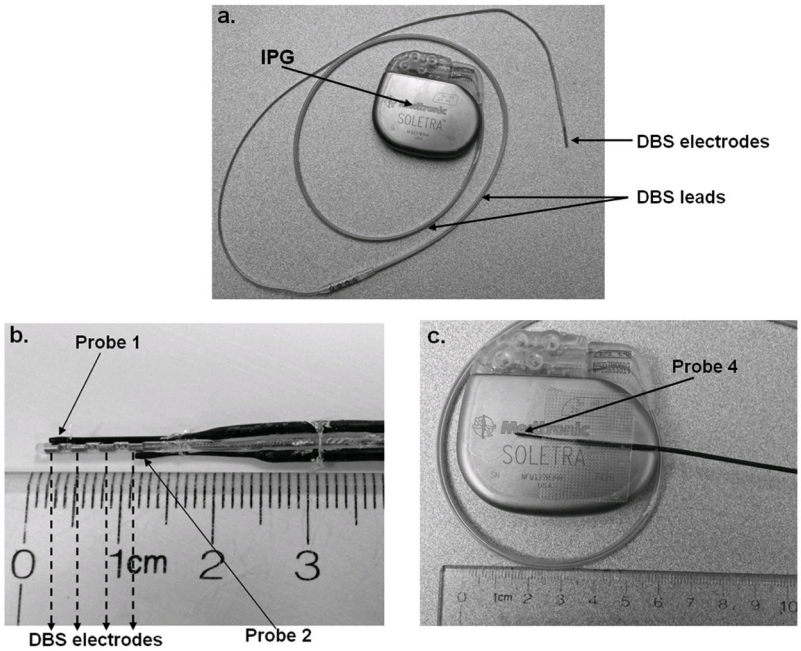

Figure 1.

Attachment of fluoroptic temperature probes to DBS electrodes and IPG: **(a)** DBS system. **(b)** Temperature probe 1 and 2 were attached directly to DBS electrodes using superglue and surgical tethers. **(c)** Probe 4 was placed on the surface of IPG using surgical tape.

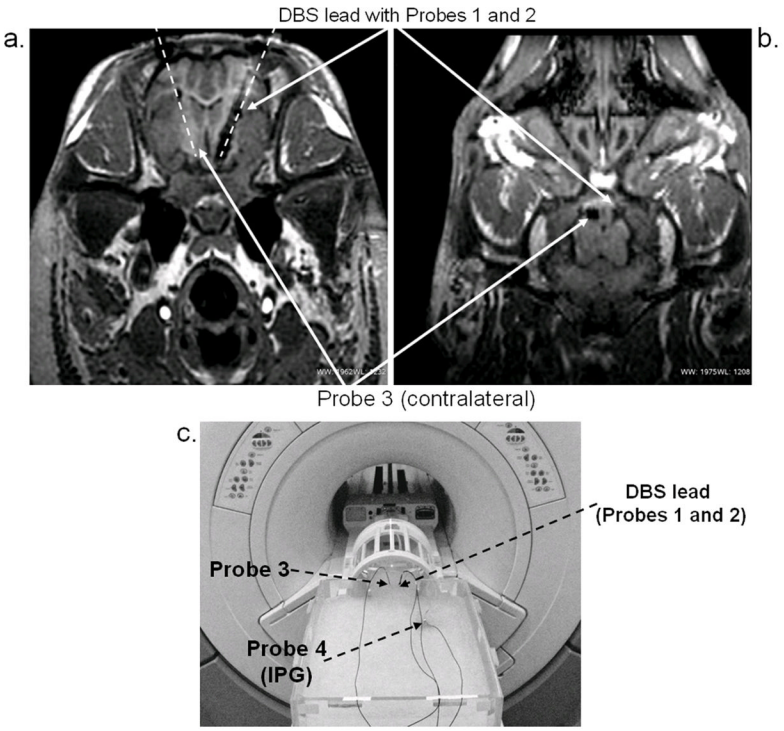

Figure 2.

Experimental setup: **(a)** Axial MR image of pig's head showing orientation and position of DBS and temperature probes (Probes 1, 2, and 3) within the STN. Overlaying dashed lines provide visual guidance. **(b)** Coronal MR image of the pig's head showing probe positions **(c)** Measurements in the head-and-trunk phantom. DBS and IPG were positioned inside the phantom in locations approximating surgical placements inside the animal.

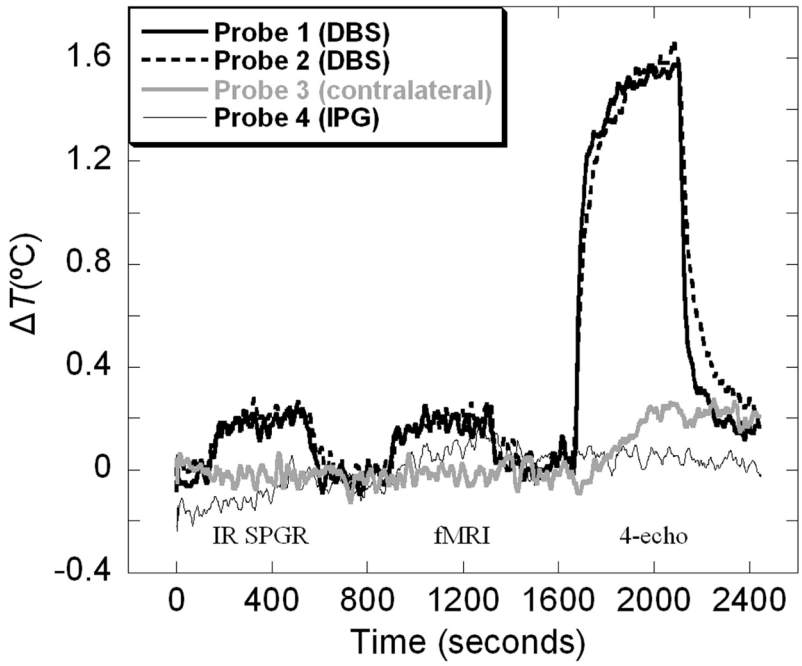

Figure 3.

Example measurement of temperature changes inside the pig's head during 3.0T MRI scanning. Temperature data shown were smooth using 20s moving average filter and corrected for slight systematic decrease of brain temperature of −0.35°C/hour due to anesthesia.

Table 1

Root-mean-squared $B^{+}_{1\,\mathrm{rms}}$ (averaged over TR) and head coil SAR (corrected for differences between human and animal anatomies) corresponding to sequences used in the experiments. The displayed and power monitor values are displayed in parentheses (subscripts D and PM, respectively). SAR_{PM} represents 6min. average displayed by the power monitor (available at 3.0T scanner only). Since the weight is arbitrarily selected for the phantom, only the corrected SAR values obtained based on auto-prescan TG are shown.

Pulse Sequence	3.0T			1.5T		
	$B_1^+{}_{rms}$ (μT)	SAR (*W/kg*)		$B_1^+{}_{rms}$ (μT)	SAR (*W/kg*)	
		Pig Study	Phantom		Pig Study	Phantom
4-echo	6.96	2.70 $(3.1)_{PM}$ $(2.9)_{C}$ $(2.2)_{D}$	3.1 $(3.1)_{PM}$	6.96	1.04 $(0.67)_{D}$	1.05
fMRI	0.30	0.41 $(0.4)_{PM}$ $(0.39)_{C}$ $(0.32)_{D}$	0.46 $(0.6)_{PM}$	0.3	0.03 $(0.02)_{D}$	0.03
IR-FSPGR	1.09	0.49 $(0.5)_{PM}$ $(0.42)_{C}$ $(0.35)_{D}$	0.47 $(0.5)_{PM}$	1.03	0.36 $(0.09)_{D}$	0.14

Table 2

3.0T in-vivo measurements of maximal temperature increases measured at the distal and proximal DBS electrodes by Probe 1 (p1) and Probe 2 (p2), respectively.

Run Number	IPG status	Geometry	Maximal temperature increases (°C)					
			4-echo		fMRI		IR SPGR	
			p1	p2	p1	p2	p1	p2
1	off	leads in coil center	1.58	1.55	0.21	0.23	0.24	0.21
2	off	leads in coil center	1.54	1.58	0.23	0.21	0.24	0.23
3	on	leads in coil center	2.0	2.0	0.29	0.22	0.25	0.23
4	on	head shifted 2 cm along z	1.78	1.82	0.21	0.29	0.24	0.31
5	on	head rotated by 3°	2.24	2.27	0.44	0.35	0.46	0.35

Table 3

Pig experiment. Maximal temperature increases ΔT_{Max} measured on the distal (Probe 1) and proximal (Probe 2) DBS electrodes during 3.0T and 1.5T scanning of the pig. The 3.0T data were averaged over two probe locations and measurement runs 1 through 5. The highest recorded values are listed below the averages. The 1.5T data were recorded during a single run and therefore individual measurements by both probes are shown.

Pulse Sequence	3.0T	1.5T
	ΔT_{Max} (°C)	ΔT_{Max} (°C)
4-echo	1.83 ± 0.28 (max = 2.27)	2.56 (p1) 2.61 (p2)
fMRI	0.27 ± 0.08 (max = 0.44)	0.17 (p1) 0.11 (p2)
IR-FSPGR	0.28 ± 0.08 (max = 0.46)	0.37 (p1) 0.28 (p2)

Table 4

Phantom experiment. Maximal temperature increases, $\Delta\ T_{Max}$, measured on DBS electrodes during 3.0T and 1.5T scanning of the ASTM head-and-torso phantom. SAR_C –average coil SAR displayed by the scanner after patient weight corresponding to auto-prescan TG was entered, SAR_{PM} – 6min. average displayed by the power monitor (3.0T).

Pulse Sequence	3.0T	1.5T
	$\Delta\ T_{Max}$ (°C)	$\Delta\ T_{Max}$ (°C)
4-echo	2.04 (p1) 1.54 (p2)	0.90 (p1) 0.81 (p2)
fMRI	0.16 (p1) 0.11 (p2)	0.12 (p1) 0.09 (p2)
IR-FSPGR	0.37 (p1) 0.24 (p2)	0.20 (p1) 0.18 (p2)

Table 5

Temperature increases measured by Probe 3 at the contralateral location during execution of the high-SAR 4-echo pulse sequence. The error bars displayed for the 3.0T in-vivo measurement are computed based on results of 5 different runs.

In-vivo pig		Phantom	
3.0T	**1.5T**	**3.0T**	**1.5T**
0.35±0.05°C	0.29 °C	0.34°C	0.17°C